Anisotropy in the Shallow Crust Observed around the San Andreas Fault Before and After the 2004 **M** 6.0 Parkfield Earthquake

by Elizabeth S. Cochran,* Yong-Gang Li, and John E. Vidale

Abstract   Local seismic arrays were deployed at two locations along the San Andreas fault (SAF) near Parkfield, California, before and after the 2004 **M** 6.0 Parkfield earthquake. Using local earthquakes we determine the anisotropic field within 1–2 km of the main trace of the SAF at the two array locations separated by 12 km. The initial array, near the SAFOD site, was deployed for six weeks in October and November 2003, and the second array, located near the town of Parkfield, was deployed for 3 months following the 28 September 2004 **M** 6.0 Parkfield earthquake.

We find the fast shear-wave polarization direction nearly fault-parallel (N40°W) for stations on the main fault trace and within 100 m to the southwest of the SAF at both array locations. These fault-parallel measurements span the 100- to 150-m-wide zone of pervasive cracking and damage interpreted from fault-zone-trapped waves associated with the main fault core (Li *et al.*, 2004, 2006). Outside of this zone, the fast orientations are scattered with some preference for orientations near N10°E, roughly parallel to the regional maximum horizontal compressive stress direction (σ_h). In addition, fast directions are preferentially oriented parallel to a northern branch of the SAF recorded on stations in the 2004 Parkfield deployment.

The measured anisotropy is likely due to a combination of stress-aligned microcracks away from the fault and shear fabric within the highly evolved fault core. The majority of our measurements are taken outside of the main fault core, and we estimate the density of microcracks from the measured delay times. Apparent crack densities are approximately 3%, with large scatter. The data suggest weak depth dependence to the measured delay times for source depths between 2 and 7 km. Below 7-km source depth, the delay times do not correlate with depth suggesting higher confining pressure is forcing the microcracks to close.

No coseismic variation in the anisotropic parameters is observed, suggesting little to no influence on measured splitting due to the 2004 **M** 6.0 Parkfield earthquake. However, the premainshock and postmainshock data presented here are from arrays separated by 12 km, limiting our sensitivity to small temporal changes in anisotropy.

Introduction

We examine crustal shear-wave anisotropy at two locations along the San Andreas fault (SAF) near Parkfield to investigate lateral and possible temporal variation in anisotropy. Local earthquake data were recorded on seismic arrays prior to and following the 28 September 2004 Parkfield **M** 6.0 earthquake. The data are from one array deployed in October and November 2003, and a second immediately after the **M** 6.0 mainshock. The 2003 array, referred to hereafter as the SAFOD array, is located adjacent to the SAFOD drilling site and the 2004 array, referred to as the Parkfield array, is located 12 km to the southeast along the main trace of the SAF (Fig. 1). During the SAFOD deployment in 2003, prior to the **M** 6.0 earthquake, the background seismicity was moderate, so we have a small but sufficient number of records to compare to the hundreds of aftershock records from 2004. The main points we address in this article are as follow: (1) the lateral variation in anisotropy along the SAF, (2) the physical cause of the observed anisotropy, and (3) the absence of a temporal change in the anisotropic parameters due to the 2004 **M** 6.0 Parkfield earthquake.

Shear-wave splitting studies have long been conducted to estimate the *in situ* stress field in the shallow crust. Shear

*Present address: Institute of Geophysics and Planetary Physics, Scripps Institution of Oceanography, University of California at San Diego, La Jolla, California 92093-0225.
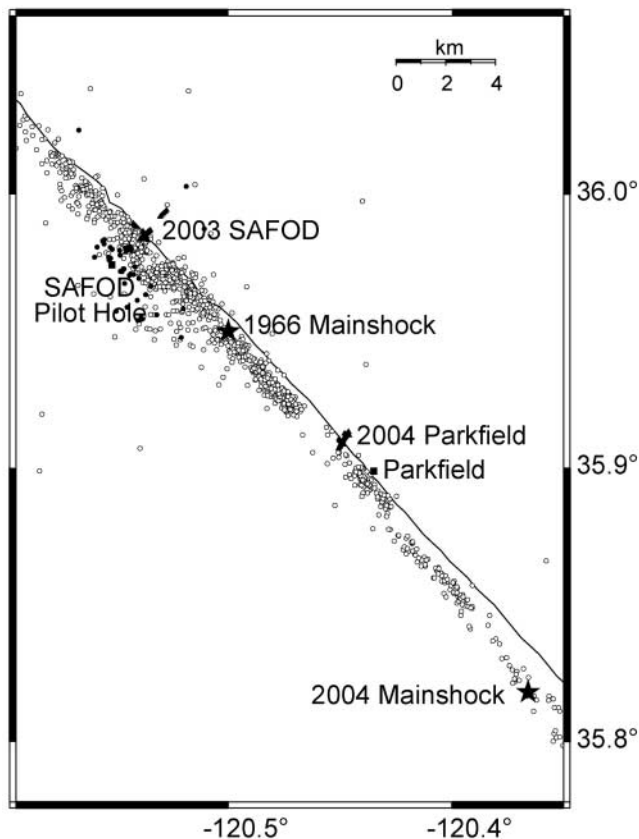
Figure 1. Map of Parkfield segment of the San Andreas fault (SAF). The 2003 and 2004 station locations are given by the filled triangles. The filled circles show earthquakes that occurred during the 2003 deployment. Aftershocks of the 2004 **M** 6.0 Parkfield earthquake that occurred during the 2004 deployment are shown by the open circles. Seismicity is likely concentrated close to the main fault plane, but catalog locations are offset to the southwest due to the large velocity contrast across the fault. The 1966 and 2004 **M** 6.0 mainshock epicenters are show by the filled stars. The town of Parkfield and the SAFOD drilling site are shown by filled squares.

waves are sensitive to compliance and wave speed that varies with polarization direction. Aligned cracks or shear fabric in the medium are the most common causes of the observed anisotropy in the upper crust (Boness and Zoback, 2004a; Crampin, 1990; Crampin and Chastin, 2003; Crampin and Zatsepin, 1997; Hudson, 1994; Zatsepin and Crampin, 1997). In the case of aligned cracks, shear-wave splitting analysis allows us to equate the fast direction with the crack orientation and the delay time with the density of cracks for each source-receiver path. Alternately, if anisotropy is due to shear fabric the anisotropic parameters relate to direction of fabric and degree of shearing. The inherent variability in anisotropic measurements requires that a significant number of records be collected to estimate the crack field or shear fabric.

Anisotropy, whether due to aligned microcracks or shear fabric, is useful to detail the structure and stress state of the fault. Aligned microcracks are thought to be sensitive to perturbations in the local stress field near an active fault and are often invoked to search for temporal changes in the stress field. Fast directions have been shown to rotate spatially, with orientations nearly fault-parallel for stations located on or very close to a fault (e.g., Peng and Ben-Zion, 2004; Tadokoro *et al.*, 1999). Analysis of focal mechanism inversions also suggest a 10° to 30° rotation in the stress field within 1–10 km from the SAF (Hardebeck and Michael, 2004; Provost and Houston, 2001; Townend and Zoback, 2004). However, the focal mechanism studies have not agreed upon the angle of the maximum local stress orientation to the strike of the SAF. The above focal mechanism inversion studies estimate that the maximum compressive stress is rotated 30° to 60° clockwise from the SAF strike in the Parkfield region.

At present, few detailed near-fault studies of the anisotropy have been conducted to search for a rotation of the stress field near an active fault. We employ two dense seismic arrays spanning 1 km and 2.4 km across the SAF to determine the orientation of the main anisotropic feature and look for lateral changes in anisotropic parameters. While the permanent array stations deployed near Parkfield provide extended temporal coverage of the anisotropic field, they cannot be used to examine 10- to 100-m spatial variations across the fault, as they are widely spaced.

A recent study by Boness and Zoback (2004a) details the anisotropic structure observed by SAFOD pilot hole stations prior to the mainshock. The multiple datasets collected in the pilot hole allow the authors to correlate the measured shear-wave splitting with observations of macrocracks, borehole breakouts, and wave speeds at depth. Boness and Zoback (2004a) suggest that the observed anisotropy is likely due to both aligned microcracks and localized shear fabric. The pilot hole is located several kilometers from the main fault strand, so they only examine the anisotropic field at one locale away from the fault. However, their study is useful to map the observed anisotropy to a physical mechanism.

Whether shear-wave splitting measurements are sensitive to changes in the local stress field during a mainshock has remained contentious. Several shear-wave splitting studies near recently ruptured fault zones have claimed to see temporal evolution of the crack field following a large magnitude earthquake or prior to earthquake swarms (e.g., Gao *et al.*, 1998; Tadokoro *et al.*, 1999; Teanby *et al.*, 2004). However, a variety surveys have seen no postseismic change in anisotropic parameters in the months following large magnitude earthquakes (e.g., Cochran *et al.*, 2003; Peng and Ben-Zion, 2004). A recent study by Boness and Zoback (2004b) of the anisotropy observed on the permanent Parkfield array stations showed no coseismic change in the anisotropy following the 2004 **M** 6.0 Parkfield earthquake. This result is somewhat surprising, given the clear coseismic changes observed in *P, S,* and trapped waves associated with

large magnitude earthquakes (Li *et al.*, 1998, 2003, 2006; Rubinstein and Beroza, 2004; Schaff and Beroza, 2004). However, a recent study by Peng and Ben-Zion (2005) suggests that shear-wave splitting studies are not sensitive to small changes in the microcrack field because the velocity change influences both the fast and slow quasipolarized shear waves. We examine the local array data for an evidence of coseismic perturbation of the observed anisotropy near the SAF due to the 2004 **M** 6.0 Parkfield earthquake.

Seismic Array Deployments

Seismic arrays were deployed along the SAF at Parkfield in two locations in 2003 and 2004. The 2003 SAFOD array was deployed near the SAFOD drilling site directly above the target earthquake locations, which are the proposed source locations to be drilled by the SAFOD project. This local seismic array was deployed to help triangulate the exact locations of the target events as well as capture the background seismicity to study the fault-zone properties. The 2004 Parkfield seismic array deployed subsequent to the **M** 6.0 mainshock was located approximately 12 km south of the SAFOD drilling site and approximately 3 km north of the town of Parkfield. The arrays were not colocated due to difficulty in permitting the SAFOD array site in 2004. Both our experiments used REFTEK recording systems with 2-Hz L22 sensors from the PASSCAL instrument center. The data were recorded at a rate of 100 samples per sec.

The 2003 SAFOD seismic array had 30 instruments deployed in a 2400-m-long cross-fault array and an additional 12 stations deployed for 400 m along the main trace of the SAF. The six-week deployment to record background seismicity was from mid-October to the end of November, 2003. The SAFOD site is located about 1 km from of the southwestern end of the cross-fault array (Fig. 1). The station spacing is irregular with a symmetric distribution across the fault, but with some gaps due to difficult field access. Station spacing near the fault is 50 m and increases to 200 m away from the fault. During the deployment, over 200 earthquakes were recorded by the array, most with magnitudes less than 2.0. Several of these events were very close to the SAFOD drilling target events and occurred almost directly under our array. These events are especially interesting as the seismic waves likely travel vertically through the fault zone and provide ideal waveforms with which to study the anisotropy of the SAF zone.

A second deployment took place in 2004 following the **M** 6.0 earthquake on 28 September 2004, referred to as the Parkfield array. The cross-fault array, in this case, has 45 three-component seismometers in an 850-m-long cross-fault and two along-fault arrays, each approximately 400 m long. The along-fault arrays were located on the main trace of the SAF which broke during the **M** 6.0 mainshock, and a secondary branch of the SAF located about 500 m north of the main trace (Fig. 1). The station spacing is 25 m in the cross-fault array and 50 m in the along-fault arrays. This deploy-

ment was operated for three months from October to December 2004 and captured almost 1000 aftershocks. An array colocated at this site was previously deployed in 2002; however, due to the very small number of earthquakes recorded (<5) at large distances from the array, no comparisons with the 2004 data could be made.

Data and Processing

In this article, we present both the 2003 SAFOD and 2004 Parkfield shear-wave splitting data to determine anisotropy near the SAF. At these locations, the seismicity tends to concentrate on or very close to the main strand of the SAF, resulting in a linear distribution of earthquakes. This limits the number of earthquakes that fall within the shear-wave window, which requires an angle of incidence of less than 45°, available to determine anisotropy parameters. However, the moderate rate of earthquakes during both deployments gives sufficient datasets to study the anisotropy. In this study, we include results for 34 earthquakes recorded in 2003 and 96 earthquakes recorded in 2004; one or more stations recorded each earthquake.

The complexity of the local geologic structure hinders accurate measurements of the shear-wave splitting. The seismograms are affected by scattered waves due to local extreme velocity contrasts across the fault (Thurber *et al.*, 2006), and many do not have the impulsive shear-wave arrivals essential for anisotropy studies. And, due to the distribution of earthquakes, the seismic waves traveling to the arrays are likely propagating nearly parallel to the main fault trace, allowing only a narrow region near the fault to be sampled. To objectively determine the anisotropy parameters, we employ an automatic program to determine the fast direction and delay time and the associated quality. With the large dataset available, it would be prohibitively time consuming to individually examine each record visually for splitting parameters.

We use the splitting program implemented by Peng and Ben-Zion (2004) that is modeled after the original code by Silver and Chan (1991). The code determines the splitting parameters using the covariance matrix method for the horizontal components and also tests the quality of the data. The data shown in this article must pass a set of 10 quality tests based on previous studies by Cochran *et al.* (2003), Gerst (2003), and Matcham *et al.* (2000) to ensure reliable and replicable shear-wave splitting measurements. Included are tests of the signal-to-noise ratio, the stability of both the fast direction and delay time over a sliding time window, and cross-correlation value, among others.

2003 SAFOD Array Results

We determined anisotropy parameters from 34 earthquakes recorded during the 6-week SAFOD deployment in 2003. The 2-km-wide dense cross-fault array provides us with a unique opportunity to study the distribution of micro-

crack orientations and densities approaching the SAF. The splitting of a shear wave can occur anywhere on the path between the source and the receiver, so we plot the data in several ways to look for systematic patterns in the data with common sources or common receivers (Fig. 2). It is likely, however, that the largest contribution is from the shallow path (e.g., Cochran *et al.*, 2003; Peng and Ben-Zion, 2004).

The high-quality splitting measurements of the fast direction and delay time for 247 earthquake–SAFOD station combinations are given in Figure 2. One or more seismic stations recorded each of the earthquakes studied, and we plot the measured splitting parameters on both the station location and source location. As is evident from the plot, significant scatter is present in the both the fast direction and delay times. The orientation of the fast-arriving shear wave is related to the orientation of the aligned crack or shear fabric that causes the splitting. If the anisotropy is caused by aligned cracks, then the fast direction aligns with the maximum compressive stress field. In addition, we might expect a strong shear fabric within the SAF core as it is a highly evolved fault system with kilometers of accumulated slip.

From the plot in Figure 2, it is evident that neither the near-source nor the near-receiver region dominates the fast orientations. Instead, the fast direction is dependent on the path, whether the path crosses the fault core, and how far the station is from the fault. Note that the earthquake locations shown in Figure 2a are likely closer to the fault plane than plotted, as the catalog locations were pulled to the

southwest by the large velocity contrast across the fault. Unfortunately, relocated earthquake locations are only available for a small subset of the data (J. Hardebeck, personal comm., 2005). In general, the fast directions measured from earthquakes that occurred directly under the array appear to show a fault-parallel preferential direction. In contrast, an event located approximately 5 km northwest of the array but still on the trace of the SAF shows nearly fault perpendicular fast directions. The earthquakes located slightly off the fault show greater scatter in the measured fast directions, most likely varying according to whether the path crosses the main fault trace.

Figures 3a and 3b plot the rose diagrams and equal area diagrams for each station of the 2003 SAFOD array for the cross and along fault arrays, respectively. The rose diagrams show the preferred fast directions measured at each station in the array. The equal area plots show how splitting results vary with source backazimuth and angle of incidence. The fast directions and delay times are highly dependent on source and received location suggesting significant fine-scale spatial variation in splitting properties.

We look in detail at the fast directions measured by stations in our along- and cross-fault arrays to determine the anisotropic parameters near the fault. Figure 4 plots rose diagrams of the distribution of fast directions for station groups. Stations were grouped based on distance from the main fault trace to determine if the splitting changes with distance from the fault.
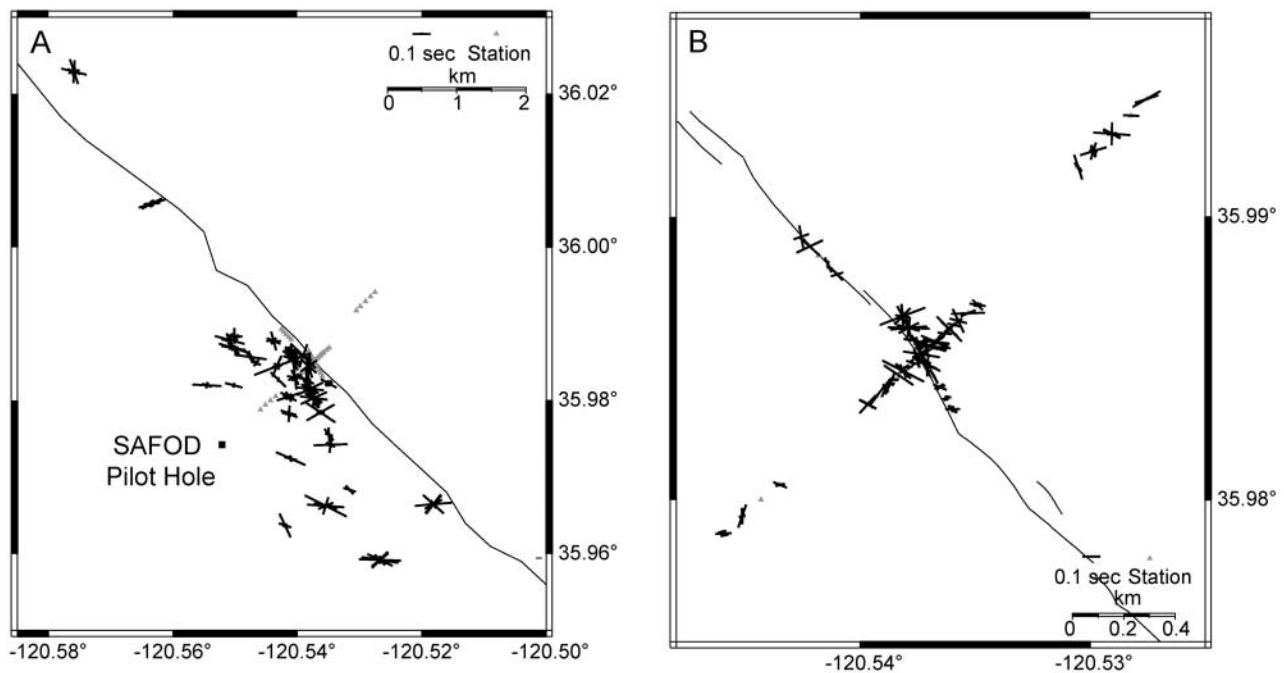

Figure 2.   Shear-wave splitting measurements from the 2003 SAFOD array. Station locations are indicated by gray triangles, and the SAF is plotted as a solid line. Bars are oriented parallel to the fast direction and scaled by the delay time. (A) Splitting results plotted on earthquake epicenter. (B) Splitting results plotted on station location. Surface trace in Figure 2B is from mapping by Rymer *et al.* (2006).
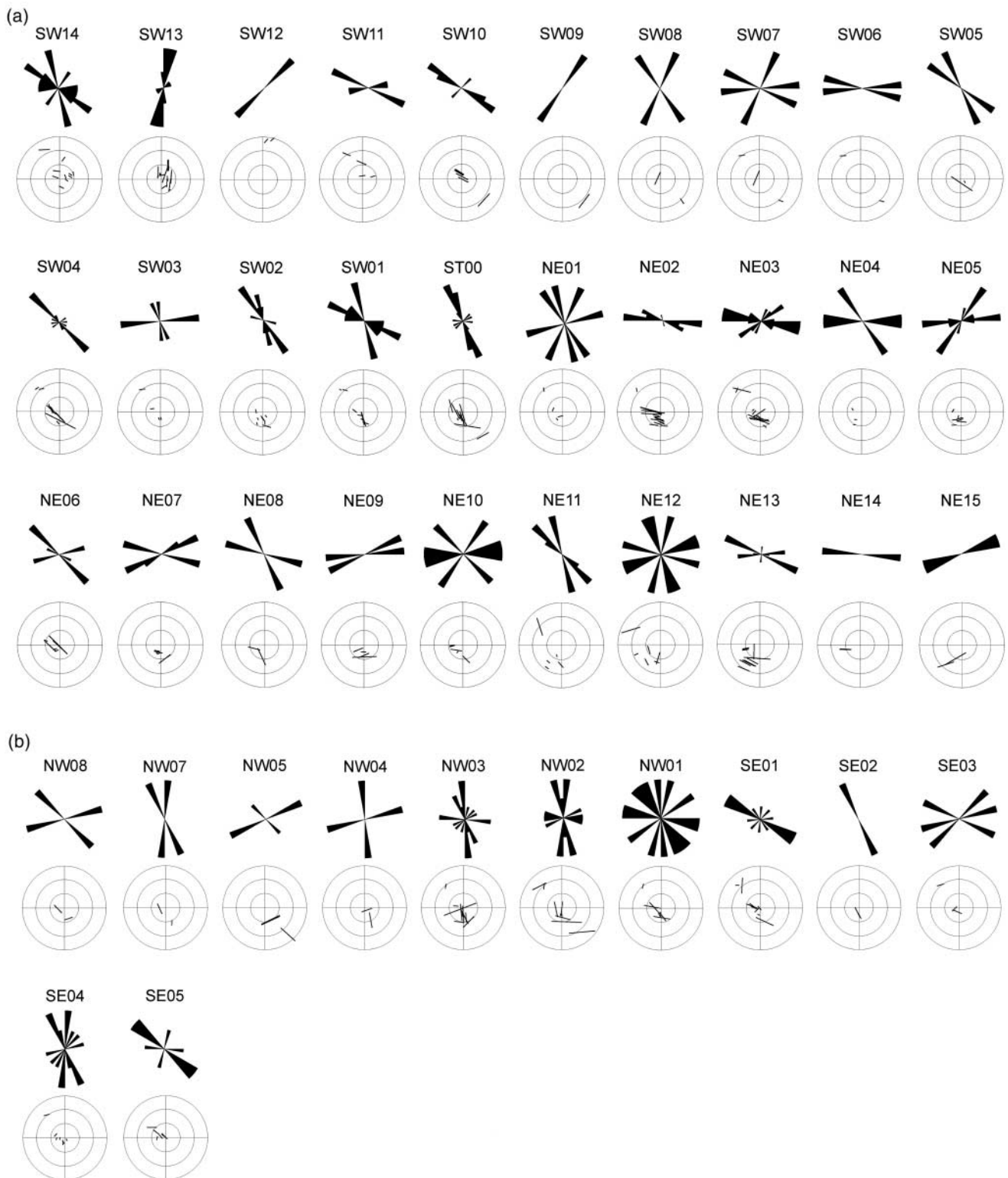
Figure 3. Rose diagrams and equal area plots of splitting parameters for each station in the 2003 SAFOD seismic array. Rose diagrams plot the polar histogram of measured fast directions only. On the equal area diagrams, splitting results are plotted on the earthquake backazimuth and angle of incidence. Bars are oriented parallel to the fast direction and scaled by delay time. Note that the radius of the equal area ranges from 0 to 45, since data processing is limited to events within the shear-wave window. (a) Results for the cross-fault stations ordered from the southwest to northeast. (b) Results for the along-fault stations ordered from the northwest to the southeast.
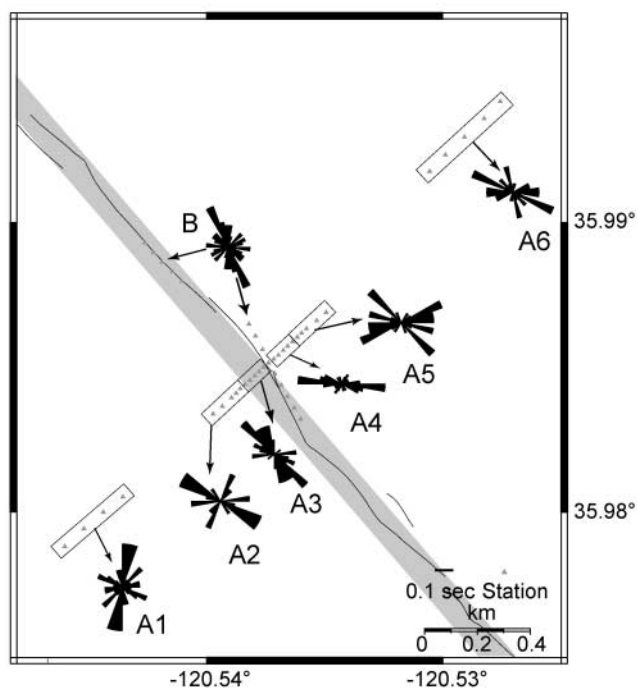
Figure 4.   Rose diagrams giving a polar histogram of the fast orientations from 2003. Fast directions are grouped by station location. Groups A (1–6) are splitting measurements from the cross-fault array, and Group B is results from the along-fault array. Gray rectangle shows the reduced velocity fault zone as determined by Li *et al.* (2006). Plotted fault trace is mapping by Rymer *et al.* (2006).

Group B, consisting of stations located on the main trace of the SAF, shows a preferential fast orientation roughly fault parallel. A similar pattern is seen for group A3 located close to the main trace on the southwest side of the fault. Away from the fault, to the southwest, the dominant direction becomes approximately N70°W for group A2. Group A1, roughly 1 km from the fault, shows directions oriented predominately N10°E. On the northeast side of the fault we see a mix of dominant fast directions from fault parallel to roughly east–west. The northeast side of the fault at the SAFOD array location has topography that may affect the accuracy of the splitting measurements due to scattered waves arriving soon after the *S* arrival. In addition, the basement rock type changes from granite to lower velocity Franciscan formation (e.g., Eberhart-Philips and Michael, 1993; Unsworth *et al.*, 1997) across the fault, likely causing scattering of the shear arrivals that may affect the measured splitting. The detailed velocity structure across the SAF near the 2003 SAFOD arrays and the possible effect on the anisotropy measurements will be discussed in more detail subsequently.

It is very common to observe large scatter in delay times measured using shear-wave splitting (e.g., Cochran *et al.*, 2003; Crampin *et al.*, 2004; Peng and Ben-Zion, 2004; Savage *et al.*, 1989; Zhang and Schwartz, 1994). Scattered delay times reflect high spatial variability in the fracture density

within the upper crust, substantial variation in shear fabric across the fault, or possibly contamination by scattering. Assuming anisotropy is constant along the source-receiver path, the average anisotropy for all of the measurements at the SAFOD array is 0.014 sec/km, with individual measurements ranging between 0.002 and 0.06 sec/km.

2004 Parkfield Array Results

Shortly after the **M** 6.0 Parkfield earthquake on 28 September 2004, we again recorded earthquakes on cross- and along-fault arrays to determine the anisotropy near the SAF at Parkfield. Although the 2003 and 2004 arrays are not co-located, they are within 12 km along a continuous section of the SAF. The fast orientations and delay times measured subsequent to the **M** 6.0 mainshock to determine whether spatial variation is similar to that observed in 2003. We looked specifically for any temporal changes in the splitting parameters that could be attributed to coseismic perturbation of the anisotropic field. Due to the high aftershock productivity following the mainshock we recorded a large number of events suitable for shear-wave splitting analysis.

Figure 5 shows splitting parameters plotted on source and receiver locations at the 2004 Parkfield array. Only the 300 high-quality results are plotted as obtained from the automated processing that pass the 10 quality factors outlined previously. We see a wide range of splitting parameters that can not be explained by purely near-source or near-receiver properties, similar to scatter seen the 2003 analysis. It is clear from the figure that there is again high spatial variability in anisotropy. In Figure 6, the rose diagrams and equal area diagrams are plotted for each station to better demonstrate the spatial distribution of the data. The rose diagrams show the dominant fast orientations measured at each station and equal area plots plot the fast direction and delay time at the propagation backazimuth and incident angle. While significant scatter is present in the results, similar source-receiver paths give similar splitting measurements, suggesting a somewhat continuous anisotropic field.

We group the fast direction data based on distance from the fault and note the average orientations (Fig. 7). The cross-fault array is split into six groups based on distance from the main and northern fault traces. We examine the fast orientations from southwest to northeast. Group A1, at a distance range of 150–250 m west of the main fault trace show orientations concentrated at near fault parallel and at N30°E. Group A2, on the southwest side of the main trace, shows predominately fault-parallel fast orientations. Group A3 has a mix of orientations, but concentrated at N20°W and N70°E. Group A4, centered between the two fault traces, the main branch of the SAF and the northern branch, shows nearly north–south fast directions. Group A5 shows a mix of fast orientations. Group A6 also has a mix of orientations, but shows fast directions parallel to the northern fault branch and fast directions nearly north–south. Both along-fault groups B and C show a mix of fast directions, but with a preferential
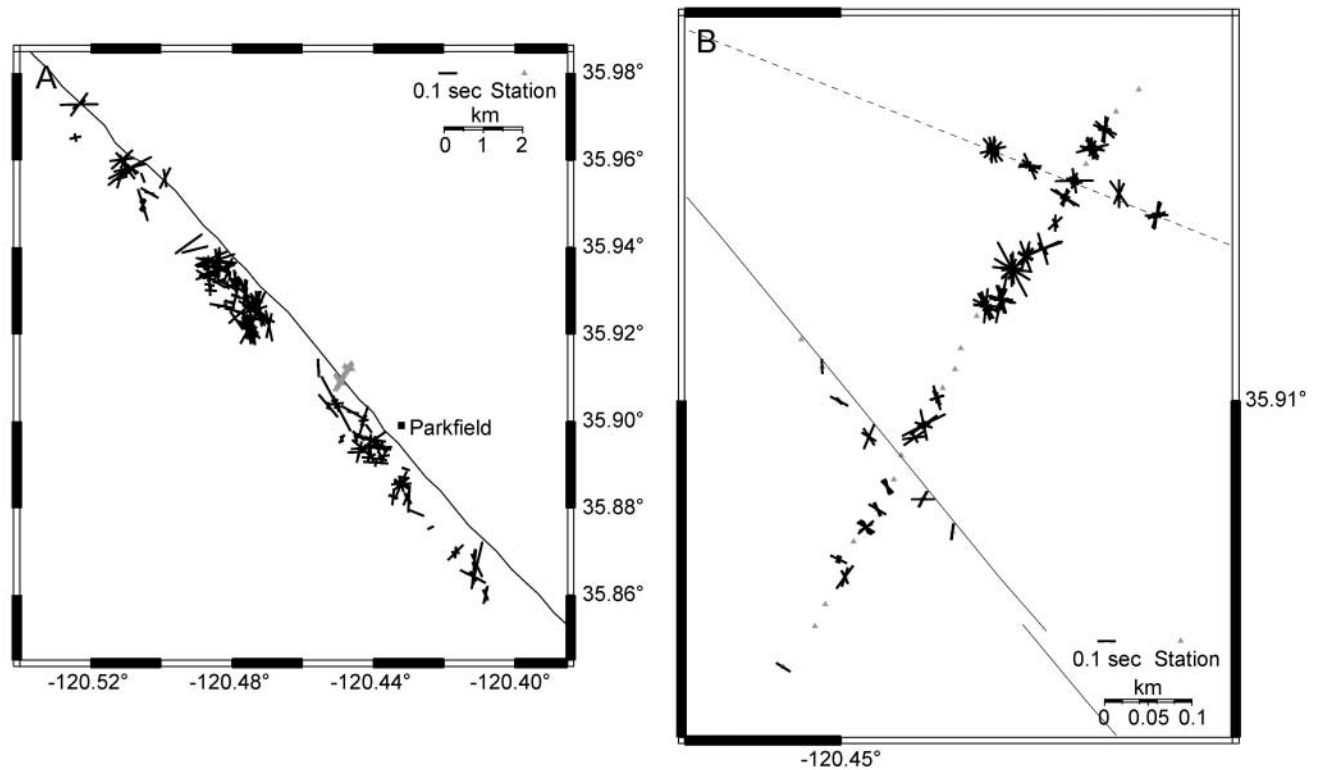
Figure 5.   Shear-wave splitting measurements from the 2004 Parkfield array. Station locations are indicated by gray triangles, and the SAF is plotted as a solid line. Bars are oriented parallel to the fast direction and scaled by the delay time. (A) Splitting results plotted on earthquake epicenter. (B) Splitting results plotted on station location.

alignment parallel to the strike of the fault. Overall, we see a pattern very similar to what was observed in 2003.

Path-normalized delay times are scattered and range from 0.002 sec/km to 0.05 msec/km. The average delay time normalized by path length for all 300 Parkfield splitting measurements is 0.012 sec/km. However, the shallowest part of the crust likely has the greatest contribution to the splitting (Cochran *et al.*, 2003; Peng and Ben-Zion, 2004), so path averaging may not be an accurate description of the delay times. Possible depth dependence will be discussed in more detail in the Discussion.

Discussion

Shear-wave splitting measurements have been used extensively to determine the anisotropic field in the shallow crust. However, due to variability in splitting measurements it can be difficult to determine the cause, location, and extent of the anisotropic body in the crust. Data recorded at two temporary array locations near the SAF prior to and following the 2004 **M** 6.0 Parkfield earthquake are analyzed to determine the characteristics of the near-fault anisotropic field. We examine the shear-wave splitting data for spatial distribution of anisotropy as well as any evidence for temporal changes due to the mainshock rupture.

The fast orientations measured by the 2003 SAFOD and 2004 Parkfield arrays show similar overall trends. The measured fast directions are oriented nearly fault-parallel for those stations located along the main trace of the SAF for both the SAFOD and Parkfield arrays. Stations at both arrays that are on the southwest side of the SAF and also within 100 m of the main trace also have fast directions that are strongly fault parallel. In addition, predominately fault-parallel fast orientations are also measured on the 2004 Parkfield array stations sited along a secondary branch of the SAF.

Outside of the fault zone, the fast directions recovered using shear-wave splitting techniques are fairly scattered. The fast orientation data for both the 2003 SAFOD and 2004 Parkfield arrays are shown in Figure 8. The 2004 Parkfield data (Fig. 8B) shows three dominant directions on the polar histogram. Two of the orientations are related to the strike of the main and northern branches of the SAF, while the third is oriented roughly N10°E. The local background stress direction has been shown to be rotated roughly 45° from the strike of the SAF, within 1–10 km of the main fault trace (Hardebeck and Michael, 2004; Provost and Houston, 2001). This would correspond to the third dominant fast orientation we see at distances of 100 m or greater from the two fault branches. In contrast, the 2003 data does not show a similar
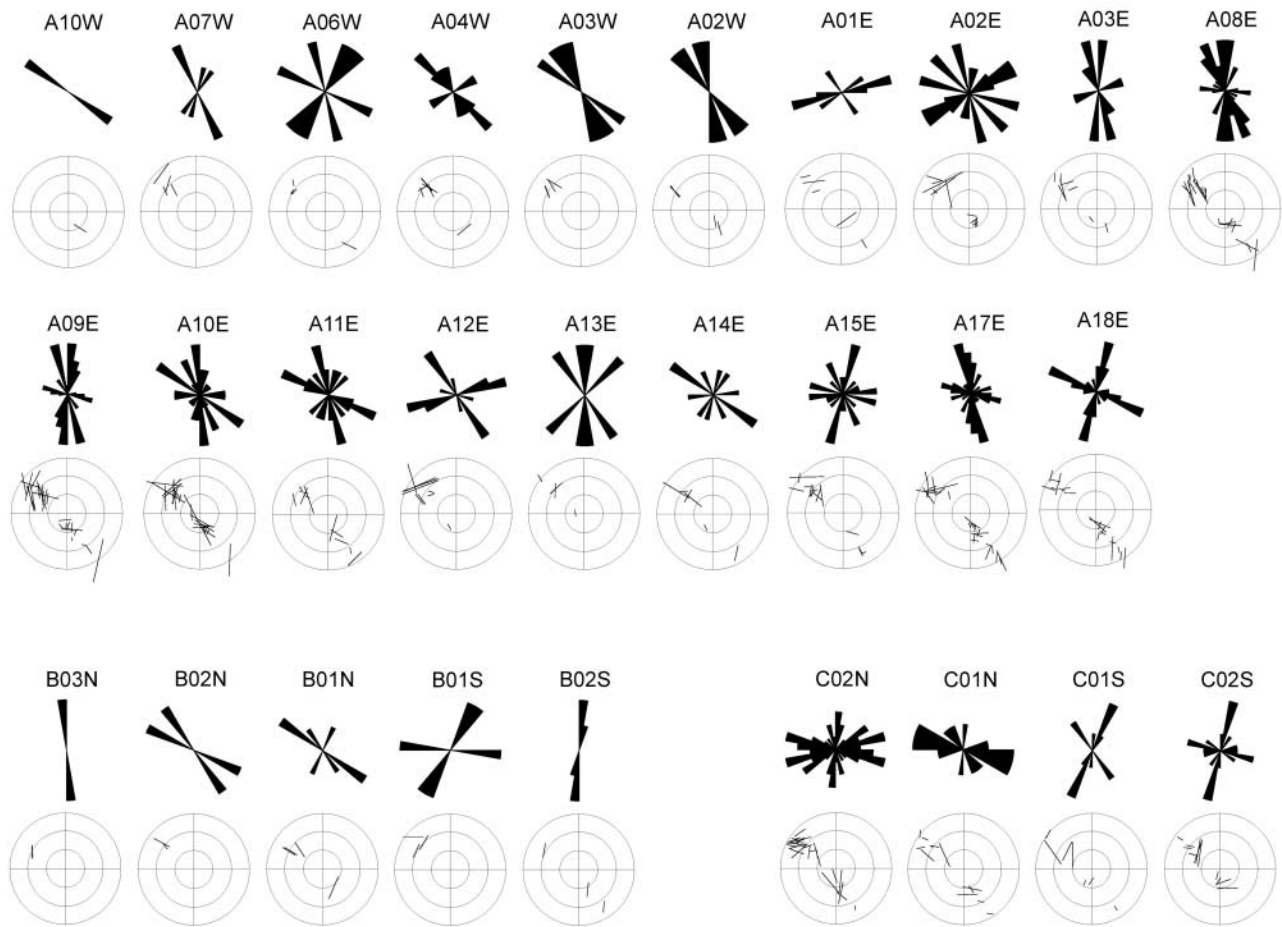
Figure 6.   Rose diagrams and equal area plots of splitting parameters for each station in the 2004 Parkfield seismic array. See Figure 3 for more detail. Stations A10W to A02W are west of the main trace of the SAF. Stations A01E to A15E are between the main trace and the northern branch of the SAF. Stations A17E and A18E are east of the northern branch. Array station names beginning with B and C are in the along-fault arrays of the main branch and northern branch, respectively.

dominant N10°E direction as shown in Figure 8a. The orientation data are more scattered and are not strongly related to the strike of the fault or the local background stress direction.

Given that the two arrays are separated by 12 km along the SAF, it is important to compare the structural and material properties of the two locations. A significant number of characterization studies have been conducted along the Parkfield segment of the SAF (e.g., Catchings *et al.*, 2002; Eberhart-Phillips *et al.*, 2003; Thurber *et al.*, 2006; Unsworth *et al.*, 1997). Structurally, both arrays span a section of the SAF that has been described as a flower structure (e.g., Catchings *et al.*, 2002) with several subsidiary branches splaying off of the main fault trace. At the Parkfield array, instruments were deployed along the main fault strand and a secondary branch to the north of the main trace. The anisotropic parameters are clearly affected by this secondary branch as stated previously.

Thurber *et al.* (2006) inverted thousands of earthquake

arrival times for the velocity structure along the SAF near Parkfield. The trait common to many of the fault-normal cross sections is a clear velocity contrast across the SAF with a 0.5–1.0 km/sec lower velocity on the northeast side of the fault compared with that on the southwest side of the fault. The velocity cross section -3 of Thurber *et al.* (2006) is colocated with our 2003 SAFOD array, and cross section 9 is close to our 2004 Parkfield array. While the two velocity cross sections are similar, there is a greater velocity contrast across the SAF at the SAFOD array. The large velocity across the fault at the 2003 SAFOD array likely causes an increase in scattered arrivals and may affect the shear-wave splitting measurements. At the 2003 SAFOD array, a clear N10°E dominant fast direction is seen for the stations farthest from the fault on the southwest side. However, no dominant fast direction is observed on the northeast side (Fig. 4).

It is often difficult to determine the cause of the observed shear-wave splitting, as there are several known physical mechanisms, including aligned microcracks, shear
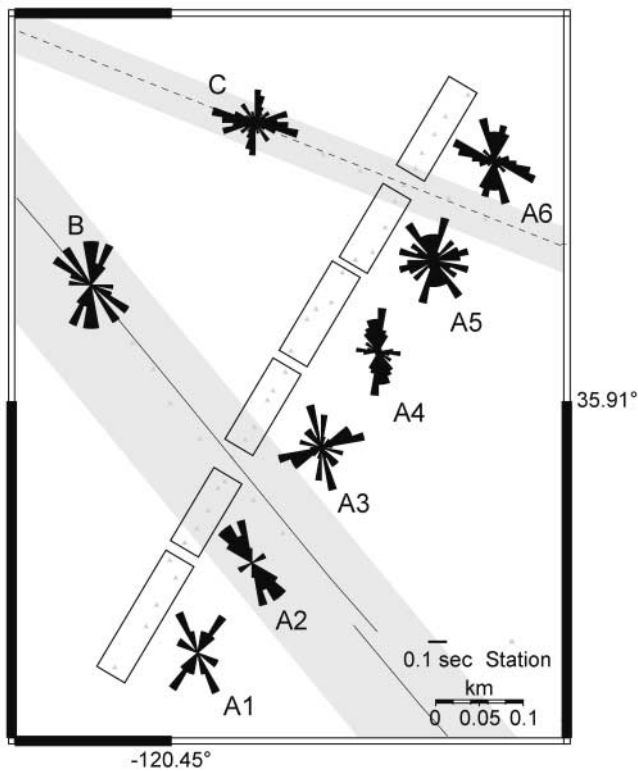
Figure 7.   Rose diagrams giving a polar histogram of the fast orientations from 2004. Fast directions grouped by station location. Groups A (1–6) are splitting orientations from the cross-fault array. Group B are the fast orientations from the along-fault array on the main trace of the SAF. Group C are those from along the northern branch of the SAF approximate location shown by a dotted line.

fabric, and preferential alignment of grains. Boness and Zoback (2004a) conducted a study of anisotropy in the SAFOD pilot hole and used a suite of borehole measurements to match the physical phenomena with the recorded shear-wave splitting. They report that the majority of splitting measurements correspond to the maximum compressive stress direction as determined from borehole breakouts, suggestive of aligned microcracks. In localized areas, anisotropy is attributed to shear fabric as seismic waves pass through highly fractured zones of slip. Therefore, we interpret that the observed anisotropy away from the main slip zones is due to aligned microcracks.

However, stations within and adjacent to the major fault traces have systematically different measured splitting orientations. There is preferential alignment parallel to the fault suggesting a strong anisotropy that could either be attributed to a shear fabric related to a highly fractured shear zone or aligned microcracks that are reoriented due to a rotation in the stress field close to the fault. Fault-zone-trapped wave studies conducted along the SAF using the same seismic array data as presented here show a strong trapping structure with reduced velocities along the fault and also to the south-

west of the fault in the width range of ~100 m (Li *et al.*, 2004, 2006). Similar to the borehole study by Boness and Zoback (2004a), the low-velocity trapping structure is associated with the strongly preferred fast direction reported here. Given the similarity between the anisotropy traits and velocity measurements measured here and in the pilot hole, we suggest that the splitting in the SAF core is likely due to shear fabric. In addition, we see no evidence of a gradual change in the fast orientations, which would be more indicative of a rotation of the stress field as the SAF is approached.

The local anisotropic field is clearly affected by the presence of the SAF, but we see little change in either fast orientations or delay times due to the 2004 **M** 6.0 mainshock. Our results are in agreement with Boness and Zoback (2004b), who reported that anisotropy results from the Parkfield permanent array stations show no evidence for a change in either fast orientation or delay time at the time of the 2004 **M** 6.0 Parkfield earthquake. It is important to note that, due to the spatial separation of our two array sites, it is difficult to definitively state that no change in the anisotropy occurred concurrent with the mainshock at these locations.

Trapped-wave data clearly indicate a decrease in the velocities in the fault core and a recovery of velocities during 3 months following the mainshock (Li *et al.*, 2006); however, we see no evidence for coseismic or postseismic changes in anisotropy parameters. The coseismic velocity decrease observed using fault zone trapped waves in the fault core is 2.5%, and recovery is on the order of 1%–2%. However, temporal variation concurrent with the Parkfield earthquake is not observed, indicating low sensitivity of anisotropy measurements to temporal changes. As reported by Peng and Ben-Zion (2005), temporal changes are observed in the direct *S*-wave and early *S*-wave coda, but the fast and slow shear-waves are affected equally, resulting in no net change in the measured shear-wave splitting.

The density of microcracks in the shallow crust, away from the fault core, is difficult to determine due to high variability in delay times measured using shear-wave splitting techniques. Figure 9 shows the delay time versus hypocentral distance and source depth for both 2003 and 2004 datasets. The largest contribution to microcrack-controlled anisotropy is from the shallow crust where confining pressures are lower and cracks can remain open. If the majority of the observed anisotropy is due to aligned microcracks, we can estimate the apparent crack density using $\varepsilon = \upsilon_s(\delta t/L)$, where ε is the apparent crack density, υ_s is the shear velocity in the uncracked medium, and $\delta t/L$ is the path-normalized delay time (Hudson, 1981; O'Connell and Budiansky, 1974). The average crack density near the SAF at both the 2003 SAFOD and 2004 Parkfield arrays is at least 3%, assuming a shear-wave velocity of 2.5 km/sec and taking the average of the path-normalized delay times. It is more likely that the anisotropy is confined to the upper 3–5 km, which would result in a greater apparent crack density in the uppermost crust than stated previously.
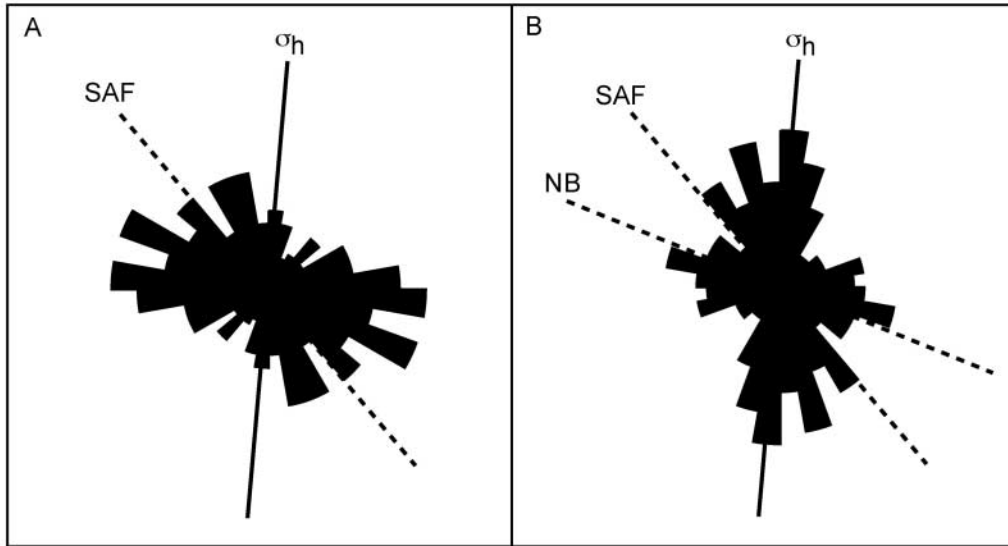
Figure 8.   Rose diagram giving the polar histogram of fast directions for (A) the 2003 SAFOD array and (B) the 2004 Parkfield array. The solid line gives the orientation of the local within 1–3 km from the fault maximum compressive stress direction (O_h) from Provost and Houston (2001). The dashed line gives the strike of the SAF and the northern branch (NB) of the SAF. Gray rectangles roughly denote the location of the reduced velocity fault zone as determined by Li *et al.* (2004).
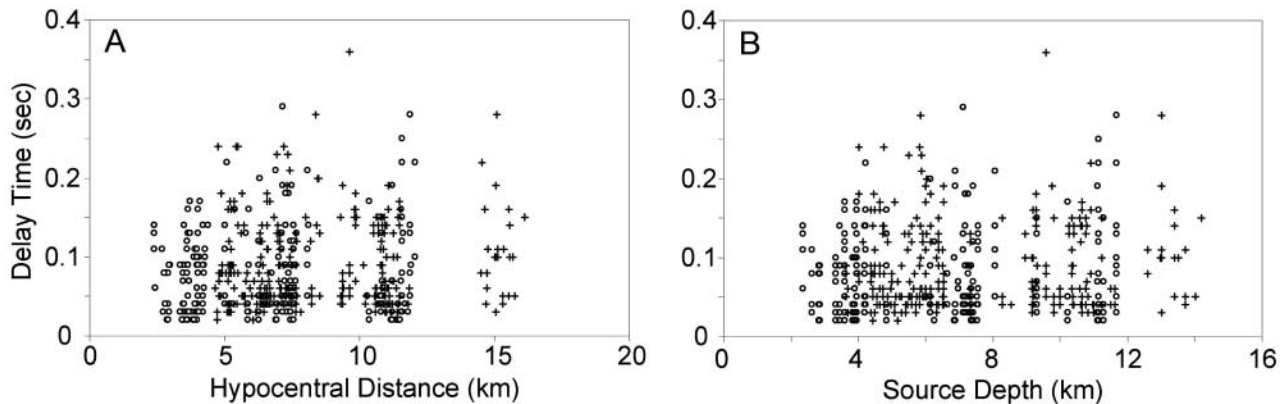

Figure 9.   Delay times from 2003 SAFOD and 2004 Parkfield seismic array data shown by circles and crosses, respectively. (A) Delay time versus hypocentral distance. (B) Delay time versus source depth.

The data are very scattered, and it is difficult to draw a conclusive statement about the depth dependence. Several studies have shown a lack of a correlation between event depth and measured delay time, suggesting that the highly anisotropic medium is confined to the upper 3–5 km (Cochran *et al.*, 2003; Peng and Ben-Zion, 2004). However, the data from all the events above 4 km show delay time less than 0.175 sec, but events at depths between 4 and 8 km show delay times up to 0.3 sec showing that the anisotropy likely persists to depth of ~7–8 km. Both Figure 9A and 9B hint at possible depth/distance dependence, but no significant correlation is evident. It is important to note that the delay times for ray paths that primarily travel through the fault core are more strongly influenced by the shear fabric.

Shear-wave splitting measurements near the SAF are highly spatially variable and clearly affected by the presence of the fault. The fast direction is fault parallel for stations directly on the fault and additionally for stations within 100 m to the southwest of the surface trace. This zone of fault-parallel fast directions overlies the region of significant velocity decrease as determined using fault-zone-trapped wave by Li *et al.* (2004, 2006). The anisotropy is likely due to aligned cracks away from the fault and shear fabric within the 100-m-wide fault zone.

Acknowledgments

References

Boness, N. L., and M. D. Zoback (2004a). Stress-induced seismic velocity anisotropy and physical properties in the SAFOD Pilot Hole in Parkfield, California, *Geophys. Res. Lett.* **31,** L15S17, doi 10.1029/2003GL019020.

Boness, N. L, and M. D. Zoback (2004b). Multi-scale crustal seismic anisotropy in the region surrounding the San Andreas fault near Parkfield, California, *EOS Trans. AGU* **85,** no. 47, Fall Meet. Suppl., T11F-05 (abstract).

Catchings, R. D., M. J. Rymer, M. R. Goldman, J. A. Hole, R. Huggins, and C. Lippus (2002). High-resolution seismic velocities and shallow structure of the San Andreas fault zone at Middle Mountain, Parkfield, California, *Bull. Seism. Soc. Am.* **92,** 2493–2503.

Cochran, E. S., J. E. Vidale, and Y.-G. Li (2003). Near-fault anisotropy following the Hector Mine earthquake, *J. Geophys. Res.* **108,** 2436, doi 10.1029/2002JB002352.

Crampin, S. (1990). The scattering of shear waves in the crust, *Pure Appl. Geophys.* **132,** 67–91.

Crampin, S., and S. Chastin (2003). A review of shear-wave splitting in the crack-critical crust, *Geophys. J. Int.* **155,** 221–240.

Crampin, S., and S. V. Zatsepin (1997). Modelling the compliance of crustal rock. II. Response to temporal changes before earthquakes, *Geophys. J. Int.* **129,** 495–506.

Crampin, S., S. Peacock, Y. Gao, and S. Chastin (2004). The scatter of time-delays in shear-wave splitting above small earthquakes, *Geophys. J. Int.* **156,** 39–44.

Eberhart-Phillips, D., and A. J. Michael (1993). Three-dimensional velocity structure, seismicity, and fault structure in the Parkfield region, central California, *J. Geophys. Res.* **98,** 15,737–15,758.

Gao, Y., P. Wang, S. Zheng, M. Wang, Y. Chen, and H. Zhou (1998). Temporal changes in shear-wave splitting at an isolated swarm of small earthquakes in 1992 near Dongfang, Hainan Island, southern China, *Geophys. J. Int.* **135,** 102–12.

Gerst, A. (2003). Temporal changes in seismic anisotropy as a new eruption forecasting tool? *MSc Thesis*, Victoria University of Wellington, Wellington.

Hardebeck, J. L., and A. J. Michael (2004). Stress orientations at intermediate angles to the San Andreas Fault, California, *J. Geophys. Res.* **109,** B11303, doi 10.1029/2004JB003239.

Hudson, J. A. (1981). Wave speeds and attenuation of elastic waves in material containing cracks, *Geophys. J. R. Astron. Soc.* **64,** 133–50.

Hudson, J. A. (1994). Overall properties of anisotropic materials containing cracks, *Geophys. J. Int.* **116,** 279–82.

Li, Y.-G., P. Chen, E. S. Cochran, J. E. Vidale, and T. Burdette (2006). Seismic evidence for rock damage and healing on the San Andreas fault associated with the 2004 **M** 6.0 Parkfield Earthquake, *Bull. Seism. Soc. Am.* **96,** no. 4B, S349–S363.

Li, Y.-G., J. E. Vidale, K. Aki, F. Xu, and T. Burdette (1998). Evidence of shallow fault zone strengthening after the 1992 M7.5 Landers, California, earthquake, *Science* **279,** 217–219.

Li, Y-G., J. E. Vidale, and E. S. Cochran (2004). Low-velocity damaged structure of the San Andreas Fault at Parkfield from fault zone trapped waves, *Geophys. Res. Lett.* **31,** L12S06, doi 10.1029/2003GL019044.

Li, Y.-G., J. E. Vidale, S. M. Day, D. D. Oglesby, and E. Cochran (2003). Postseismic fault healing on the rupture zone of the 1999 M7.1 Hector Mine, California, earthquake, *Bull. Seism. Soc. Am.*, **93,** 854–869.

Matcham, I., M. K. Savage, and K. R. Gledhill (2000). Distribution of seismic anisotropy in the subduction zone beneath the Wellington region, New Zealand, *Geophys. J. Int.* **140,** 1–10.

O'Connell, R. J., and B. Budiansky (1974). Seismic velocities in dry and saturated cracked solids, *J. Geophys. Res.* **79,** 5412–5426.

Peng, Z., and Y. Ben-Zion (2004). Systematic analysis of crustal anisotropy along the Karadere-Düzce branch of the North Anatolian Fault, *Geophys. J. Int.* **159,** 253–274.

Peng, Z., and Y. Ben-Zion (2005). Temporal changes of shallow seismic velocity around the Karadere-Düzce branch of the north Anatolian fault and strong ground motion, *Pure Appl. Geophys.* "Advances in Studies of Heterogeneities in the Earth's Lithosphere: The Keiiti Aki Volume II" **163,** 567–599, doi 10.1007/s0002400500346doi.

Provost, A.-S., and H. Houston (2001). Orientation of the stress field surrounding the creeping section of the San Andreas fault: evidence for a narrow mechanically weak fault zone, *J. Geophys. Res.* **106,** 11,373–11,386.

Rubinstein, J. L., and G. C. Beroza (2005). Depth constraints on nonlinear strong ground motion, *Geophys. Res. Lett.* **32,** L14313, doi 10.1029/2005GL023189.

Rymer, M. J. (2006). Surface fault slip associated with the 2004 Parkfield, California, earthquake, *Bull. Seism. Soc. Am.* **96,** no. 4B, S11–S27.

Savage, M. K., X. R. Shih, R. P. Meyer, and R. C. Aster (1989). Shear-wave anisotropy of active tectonic regions via automated shear-wave polarization analysis, *Tectonophysics* **165,** 279–292.

Schaff, D. P., and G. C. Beroza (2004). Coseismic and postseismic velocity changes measured by repeating earthquakes, *J. Geophys. Res.* **109,** B103002, doi 10.1029/2004JB003011.

Silver, P. G., and W. W. Chan (1991). Shear-wave splitting and subcontinental mantle deformation, *J. Geophys. Res.* **96,** 16,429–16,454.

Tadokoro, K., M. Ando, and Y. Umeda (1999). S-wave splitting in the aftershock region of the 1995 Hyogo-ken Nanbu earthquake, *J. Geophys. Res.* **104,** 981–991.

Teanby, N., J.-M. Kendall, R. H. Jones, and O. Barkved (2004). Stress-induced temporal variation in seismic anisotropy observed in microseismic data, *Geophys. J. Int.* **156,** 459–466.

Thurber, C., H. Zhang, F. Waldhauser, J. Hardebeck, A. Michael, and D. Eberhard-Phillips (2006). Three-dimensional compressional wave-speed model, earthquake relocations, and focal mechanisms for the Parkfield, California, region, *Bull. Seism. Soc. Am.* **96,** no. 4B, S38–S49

Townend, J., and M. D. Zoback (2004). Regional tectonic stress near the San Andreas fault in central and southern California, *Geophys. Res. Lett.* **31,** L15S11, doi 10.1029/2003GL018918.

Unsworth, M. J., P. E. Malin, G. D. Egbert, and J. R. Booker (1997). Internal structure of the San Andreas fault at Parkfield, California, *Geology* **25,** 359–362.

Wessel, P., and W. H. F. Y. Smith (1998). New, improved version of the Generic Mapping Tools released, *EOS Trans. AGU* **79,** 579.

Zatsepin, S. V., and S. Crampin (1997). Modelling the compliance of crustal rock. I. Response of shear-wave splitting to differential stress, *Geophys. J. Int.* **129,** 477–494.

Zhang, Z., and S. Y. Schwartz (1994). Seismic anisotropy in the shallow crust of the Loma Prieta segment of the San Andreas fault system, *J. Geophys. Res.* **99,** 9651–9661.

Earth and Space Sciences Department and Institute of Geophysics
    and Space Physics
University of California
Los Angeles, California 90095-1567
    (E.S.C., J.E.V.)

Department of Earth Sciences
University of Southern California
Los Angeles, California 90089-0740
    (Y-G.L.)